Analysis of the Endwinding Cooling Effects in TEFC Induction Motors

Analysis of the Endwinding Cooling Effects in TEFC Induction Motors

Aldo Boglietti, *Senior Member, IEEE*, and Andrea Cavagnino, *Member, IEEE*

***Abstract*—This paper deals with the endwinding cooling problems of totally enclosed fan-cooled (TEFC) induction motors. In order to obtain information about the phenomena involved in the motor end space, three "*ad hoc*" prototypes have been build. The complete test-bench setup, together with the followed test procedures, is reported in detail. The measurement results have shown that all the motor-part overtemperatures (winding, endwindings, stator lamination, and external motor frame) decreasing, with the inner air speed increasing. The measured motor overtemperatures and losses allow the thermal-resistance identification of a simplified thermal model suitable to describe the thermal behaviors of the prototypes. By the endwinding-to-motor frame thermal resistance, the related heat-exchange coefficients have been evaluated as a function of the rotor speed. The proposed procedure allows separating the forced-convection contribution by the other thermal-exchange phenomena that occur in the end-space regions. The obtained heat-transfer coefficients are in agreement with the results reported in the past literature.**

***Index Terms*—Endwinding cooling, forced-convection heat exchange, thermal analysis, totally enclosed fan-cooled (TEFC) induction motors.**

I. Introduction

THE ENDWINDINGS are typically the hottest points inside a totally enclosed fan-cooled (TEFC) induction motor. A more efficient endwinding cooling allows decreasing the thermal solicitations of the windings with better reliability of the motor or, on the other hand, an increase of the produced steady-state torque with the same imposed overtemperature. The aluminum die-cast process, typically used for the squirrel-cage production, allows producing short-circuit rings with several wafters, fins, or tips, which create air whirls inside the motor end-caps. This air movement increases the forced-convection heat transfer between the endwindings and the motor end-caps. The turbulent airflow inside the end-caps depends on several factors such as the shape and the length of the stator endwindings and the shape and number of wafters, fins, and tips always present on the short-circuit rings [4].

Paper IPCSD-07-022, presented at the 2006 Industry Applications Society Annual Meting, Tampa, FL, October 8–12, and approved for publication in the IEEE Transactions on Industry Applications by the Electric Machines Committee of the IEEE Industry Applications Society. Manuscript submitted for review October 31, 2006 and released for publication March 22, 2007. This work was supported by the Ministero dell'Istruzione Università e Ricerca COFIN2005.

The authors are with the Dipartimento di Ingegneria Elettrica, Politecnico di Torino, 10129 Turin, Italy (e-mail: aldo.boglietti@polito.it; andrea.cavagnino@polito.it).

Color versions of one or more of the figures in this paper are available online at http://ieeexplore.ieee.org.

Digital Object Identifier 10.1109/TIA.2007.904399

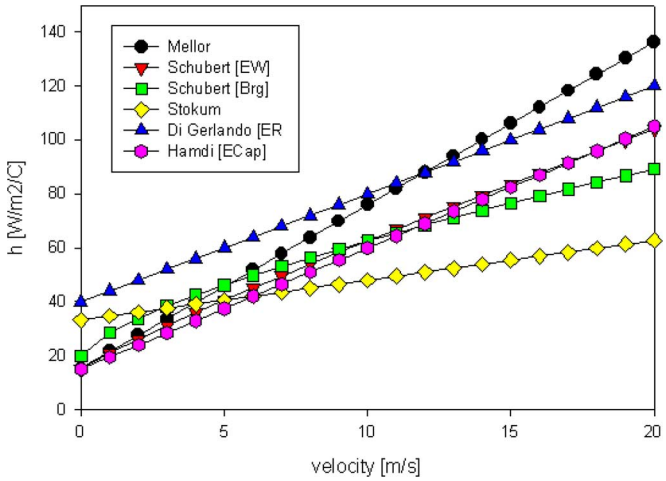

Fig. 1. Published correlations for the equivalent heat-exchange coefficients in the end regions for TEFC induction motors.

The heat-transfer phenomena in the end region of TEFC induction motors have been subject of studies by several authors, which proposed the use of a general formulation for the related heat-transfer coefficient [1]–[3], [8]–[10], hereafter reported, where "v" is the inner air speed in meters per second

$$h = k_1 \left[1 + k_2 v^{k_3}\right]. \tag{1}$$

The related values of K_1, K_2, and K_3 are reported in [11]. The inner air speed is the speed of the air in the end-cap regions when the rotor is running. Due to the endwindings, end-caps, and short-circuit rings geometry, the selection of a representative value of the inner air speed is not a simple task, as discussed in [4]. From the practical point of view, in (1), the rotor peripheral speed is usually adopted [4].[1]

Fig. 1 shows the published correlation between the heat-transfer coefficients as a function of the inner air speed [5].

As shown in (2), an accurate value of the heat-transfer coefficient is requested to evaluate the thermal resistance $(R_{\rm th})$ related to the thermal exchanges between a surface (i.e., the endwinding surface) and the inner air.

$$R_{\rm th} = \frac{1}{hS}. \tag{2}$$

In (2), h is the heat-transfer coefficient measured in Watts per square meter per degree Celsius, and "S" is the surface involved by the phenomenon measured in square meters. Due to

[1] [Online]. Available: www.motor-design.com.

the geometry of the endwinding and end-caps, the computation of the surface "*S*" in not simple.

The problems linked to a correct endwinding-cooling thermal model in electrical machine can be still considered an open problem. Taking into account the publication years, several papers are dated, while the processes to build induction motor are changed with the technological evolution, in particular, from the winding-insulation point of view.

This means that, for the prototypes under study, a better insulation thermal conductivity is probable. In addition, it is also probable that the rotors used in the previous studies should be wound rotors, without fins and tips that can improve the inner air ventilation. It is important to highlight that some papers show just the obtained results without reporting the methodology used to get them.

It is important to observe that the heat-transfer coefficient (1) has to be considered as an "equivalent" coefficient because it takes into account all the heat-exchange phenomena that occur in the end-space region. In particular, (1) includes the natural-convection and the radiation phenomenon when the rotor is still, and the natural convection, the radiation, and the forced-convection phenomenon when the rotor is running. As proof of this fact, it is possible to observe that the correlations reported in Fig. 1 do not cross the axis origin when the rotor is still.

In this paper, three "*ad hoc*" motor prototypes have been used to measure the thermal exchange between the stator endwindings and the motor frame. Several tests have been performed, and the obtained results have led to interesting information useful for improving the thermal model of the stator endwindings. In particular, the proposed simplified thermal model allows calculating the involved thermal resistances and the related heat-transfer coefficients. Finally, on the base of suitable hypothesis, the forced-convection heat exchanges involved in the air space inside the motor end caps, when the rotor is in rotation, have been analyzed.

II. Description of the Prototypes

The thermal analysis of an electrical motor is a complex problem where a great number of thermal-exchange phenomena are involved. In fact, conduction, natural convection, forced convection, and radiation are all present, with a weight that depends on the motor cooling system (natural convection, fan cooling, water cooling, etc.). The most used procedure for analyzing the electrical-machine thermal behaviors is usually based on thermal network with lumped parameters. A lot of paper can be found in the technical literature on this subject [6]–[8], [11].

Unfortunately, the weak point of this approach is the correct thermal-resistance computation. In particular, the thermal resistances linked to the forced convection and the radiation heat exchanges are very difficult to evaluate with an acceptable accuracy. In fact, even if the geometrical quantities are known, the correct evaluation and choice of the heat-transfer coefficients is not a simple task, and it requires a good skill to manage these problems. In order to better identify the phenomena involved in the endwinding cooling, it is important to define a system where only the stator joule losses are active, while the other thermal sources must not be present. This choice is reasonable for the following reasons.

1) The endwindings represent the motor parts mainly influenced by the inner air whirls.
2) With sinusoidal supply, the loss-contribution values are not known with a very good accuracy (the loss separation is made following international standards).
3) The thermal system is much plain, and a simplified thermal network can be adopted and set up on the base of the experimental tests [6], [12].

For this reasons, three "*ad hoc*" prototypes have been built. The prototypes are base on standard TEFC motors, where the rotor lamination and rotor squirrel cage has been replace by a plastic cylinder. In order to keep on the internal ventilation effect, the two end-rings of the original rotors have been fixed on the two sides of the plastic cylinder. The plastic-rotor diameter is obviously equal to the original one. The adopted motor code, together with the main geometrical data of the three prototypes, is reported in Table I. Just for example, Fig. 2 shows the original rotor and the "plastic" rotor for the MA160 prototype.

The prototypes are thermally monitored with PT100 sensors. In particular, three sensors have been positioned inside the endwindings (one for each phase), and a sensor is positioned in a hole drilled in the stator lamination. For the MA160 prototype, an additional thermal sensor is positioned inside a stator slot.

TABLE I
Main Geometrical Data of the Prototypes

Motor prototype	MA160	MA132	MA112
Original motor rated power [kW]	11	7.5	4
Rotor diameter [mm]	131	111	111
Axial core length [mm]	210	190	126
Endwinding length [mm]	155	162	147
Endwindings length / average coil length	0.42	0.46	0.54
Endwinding perimeter [mm](*)	110	105	100
Endwinding average diameter [mm] (*)	175	150	140
Endwinding to end caps distance [mm] (*)	50	15	15

(*) See Fig. 3.c. The endwinding perimeter is the endwinding axial section perimeter.

Fig. 2. Example of the original and "plastic" rotor (MA160 motor) with the short-circuit ring detail (for all the prototypes, there are 12 fins and tips on the ring).

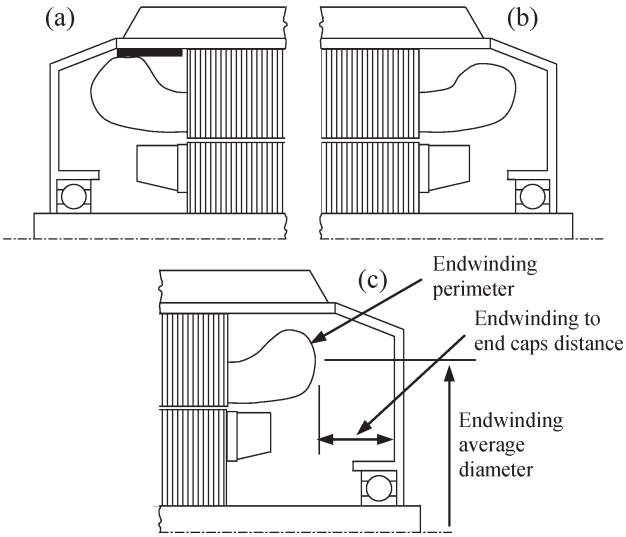

Fig. 3. Sketch of the end-space regions of the motor prototypes.

Fig. 3 depicts the different extension of the endwindings in the end-space region. The following aspects have to be underlined.

1) For the MA112 prototype, the shaft-side endwinding [Fig. 3(a)] has the same geometrical shape of the cooling-fan-side one [Fig. 3(b)], but in the shaft side, the endwinding is in contact with the external frame by an insulation cap of 1-mm thickness [shown in black in Fig. 3(a)]. This means that there is a conduction thermal path between the shaft-side endwinding and the motor frame. In addition, Fig. 3(a) and (b) shows that the two endwindings are inside the end-cap space.
2) For the MA132 prototype, the two endwindings (shaft side and cooling fan side) are symmetrical, and their geometry is sketched in Fig. 3(b). In addition, for this motor, the endwindings get in inside the end caps.
3) For the MA160 prototype, the two endwindings are symmetrical [Fig. 3(c)], and they do not get in inside the end-cap regions.

For the three prototypes under study, the shape and number of fins and tips present on the short-circuit rings are equal, and the endwinding geometries are quite similar. Table I shows that the ratio between the endwindings length and the average coil length is different. On the base of all previous considerations, it is reasonable to conclude that the inner ventilation effects could be different for the three prototypes.

III. Experimental Test Procedures

The prototype has been mechanically connected to a synchronous motor that puts in rotation the plastic rotor (Fig. 4). The synchronous motor is driven at variable speed by a three-phase sinusoidal static generator that is regulated in frequency and voltage. In order to avoid forced ventilation on the external motor frame, the fan of the prototype and the fan of the synchronous motors have been removed.

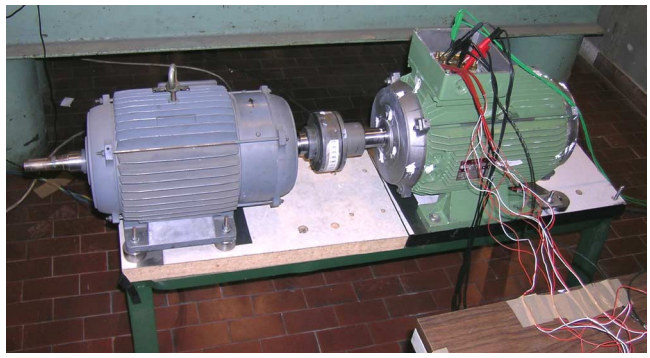

Fig. 4. Test-bench setup: (right) motor prototype under test and (left) synchronous motor.

As proposed in the study in [12], using a dc supply for the prototype stator winding, the following test conditions are obtained:

1) stator joule losses active;
2) iron losses nonactive (stator dc supply);
3) rotor joule losses nonactive (plastic rotor);
4) friction losses in the bearing active but negligible with respect to the stator joule losses;
5) variable rotor-speed condition.

Neglecting the bearing losses, it is well evident that only the stator winding is active as thermal source. As a consequence, with respect to a still-rotor condition, temperature variations of the stator winding when the rotor is running have to be attributed to the inner forced-ventilation effects.

With the stator winding supplied by a dc current, several tests have been performed with rotor-speed variable for 0–2400 r/min. All the tests have been done with the three motor phases connected in parallel, and since the forced ventilation is nonactive on the motor external frame, a reduced dc current has been used in order to avoid winding damage. In particular, a constant electric power of 200, 170, and 140 W has been respectively considered for the MA160, MA132, and MA112 motor prototypes.

For each considered rotor speed and with the prototype in steady-state thermal condition, the temperatures (by the thermal sensors), the average external frame temperature (measured on 25 points on the motor-frame surface), the applied dc power, and the winding resistance have been measured.

IV. Experimental Results

A. MA160 Motor Prototype

In Fig. 5, the average winding overtemperature (evaluated by the winding-resistance value) as a function of the rotor speed is reported. As usual, the overtemperature is evaluated with respect to the ambient one. In the same figure, the overtemperature of the stator lamination and the external motor frame are also shown. With respect to the still-rotor condition, the overtemperature reduction of each machine parts is well evident. This reduction is due to the forced-convection thermal exchange in the inner air when the rotor is rotating. In particular, it is possible to observe a linear overtemperature decrement

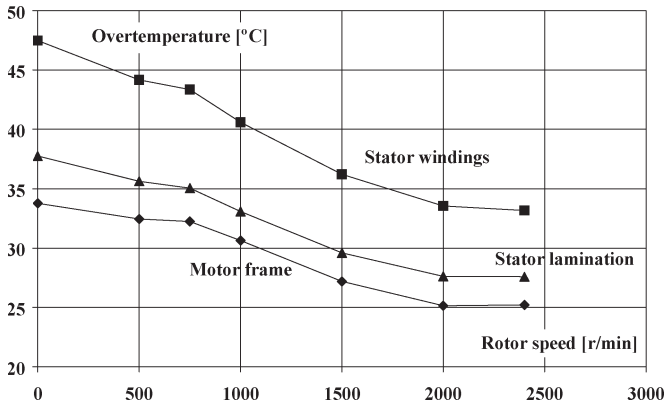

Fig. 5. MA160 prototype: average stator winding, stator lamination, and motor external-frame overtemperature versus the rotor speed.

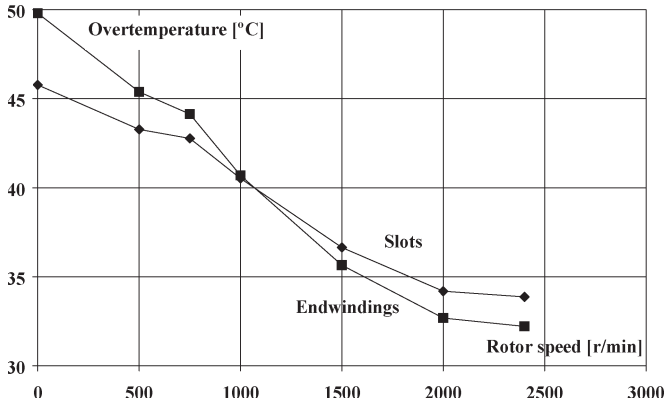

Fig. 6. MA160 prototype: overtemperature of different parts of the stator winding versus the rotor speed.

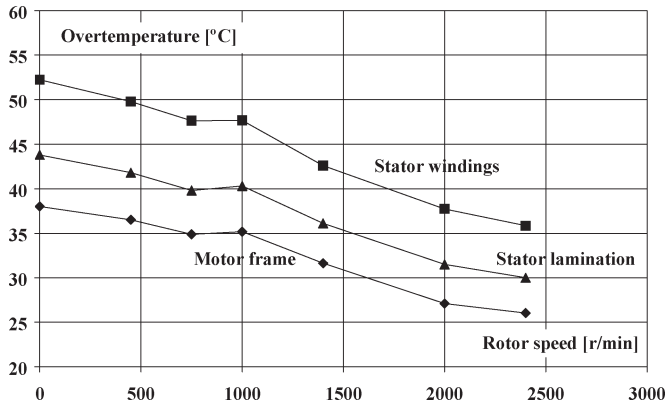

Fig. 7. MA132 prototype: average stator winding, stator lamination, and motor external-frame overtemperature versus the rotor speed.

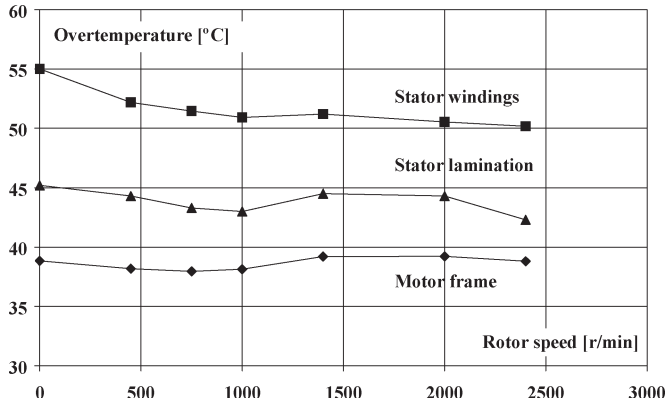

Fig. 8. MA112 prototype: average stator winding, stator lamination, and motor external-frame overtemperature versus the rotor speed.

with rotor speed in the range of 0–1000 r/min and a hyperbolic trend for speed higher than 1000 r/min.

Fig. 6 shows the overtemperature of the stator-winding part embedded in the slots and the endwinding overtemperature versus the rotor speed. It is interesting to observe that, when the rotor speed is zero, the endwinding temperature is higher than the slot copper one, whereas at high speed, the endwindings is colder than the slots. This result is reasonable, taking in to account the ventilation effect, due to the wafters present on the rotor short-circuit rings.

On the basis of this consideration, it is possible to conclude that there is a heat transfer between the copper embedded in the slots and the copper of the endwindings and that the direction of this heat flux depend by the rotor speed.

It is interesting to observe that the average winding overtemperature evaluated by the data reported in Fig. 6 (taking into account the endwindings length and the axial length of the slots) is equal to the overtemperature calculated by the winding resistance in thermal steady-state conditions. This means that the temperature measurements provided by the thermal sensors buried in the winding can be considered accurate.

B. MA132 Motor Prototype

For this motor prototype, the thermal sensor in the slot is not available. The measurements have highlighted that, in the whole speed range, the difference between the average endwinding temperature (measured with the PT100 sensor) and the average winding temperature (evaluated by the steady-state winding-resistance value) is lower than 1 °C. As a consequence, for the endwindings and for copper embedded in the slots, the same temperature has been considered (equal to the average of two previous measurements).

The average stator winding, stator lamination, and the external motor frame overtemperatures versus the rotor speed are reported in Fig. 7. Because the obtained trends for the different motor-part temperatures are very similar to those measured for the MA160 (Fig. 5), the same considerations can be done.

C. MA112 Motor Prototype

For this motor, the measurement results show that the endwinding temperature, and the average winding temperature are very close in the whole speed range (difference lower than 0.8 °C). In addition, in this case, the endwindings and the copper in the slot have been considered at the same average temperature.

The overtemperatures of the different motor parts versus the rotor speed are reported in Fig. 8.

Fig. 8 shows a different thermal behavior of this prototype with respect to the other two. For all the MA112 motor parts,

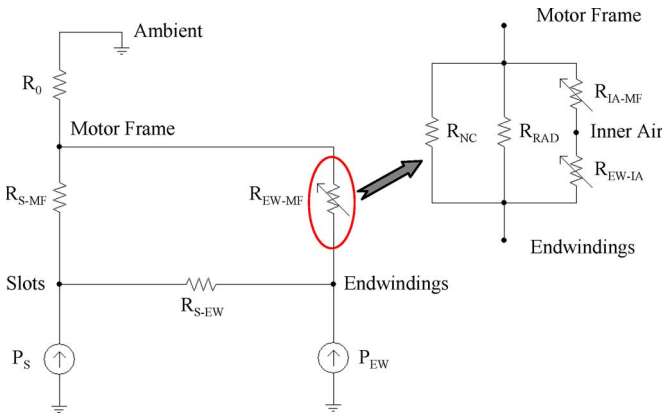

Fig. 9. Proposed simplified thermal model for the prototype.

a linear temperature decreasing between 0 and 1000 r/min has been obtained, but for speed higher than 1000 r/min, it is possible to observe a small temperature increase for the stator lamination and the motor external frame. In any case, the winding temperature continues to decrease, also at high speed.

On the base of the considerations reported in the previous section related to the MA112 prototype [Table I, Fig. 3(a) and (b)], it is reasonable to conclude that the inner cooling effects could not be so efficient when the rotor is running at high speed. In fact, for this motor, the clearance between the endwindings and the end-caps and between the endwindings and the frame is quite narrow, and as a consequence, the cooling effect due to the airflow produced by the fins is reduced.

In addition, it is important to observe that the influence of the mechanical losses (the only loss term not under control in the tests) could be not negligible at high speed since the MA112 is the smallest prototype under study and the dc power injected in the tests is also the smaller one.

V. Simplified Thermal Model

Starting from the thermal model proposed in [6], it is possible to define a simplified thermal model, which describes the thermal behaviors of the motor prototypes under study. Since the rotors are realized in plastic, the heat flux in the airgap–rotor-shaft thermal path can be neglected for any rotor-speed condition. Due to the temperature difference between the endwindings and the copper embedded in the slots measured in the MA160 motor prototype, a thermal resistance between these two winding parts has to be considered in the proposed thermal model.

On the base of these considerations, the thermal network shown in Fig. 9 has been adopted. The meanings of the parameters are enumerated in the following:

1) R_0: natural-convection thermal resistance between the external-motor frame and the surrounding ambient;
2) $R_{S-\mathrm{MF}}$: equivalent thermal resistance between the copper embedded in the slots and the motor frame;
3) $R_{S-\mathrm{EW}}$: thermal resistance between the copper inside the slots and the endwindings;
4) $R_{\mathrm{EW}-\mathrm{MF}}$: equivalent thermal resistance between the endwinding and the motor frame;
5) P_S: power losses in the winding part inside the slots (taking into account the actual temperature);
6) P_{EW}: power losses in the endwindings (taking into account the actual temperature).

The R_0 resistance can be calculated as the temperature difference between the motor frame and the ambient divided by the total power loss in the stator winding. The R_0 resistance includes the natural convection and radiation thermal exchange. As a consequence, even if the main forced convection over the external frame is not present, this resistance is not constant because it depends on the actual motor frame and ambient temperature. In addition, due to the shaft rotation, some small and parasitic external forced ventilation are present. It is interesting to underline that, with the rotor running at high speed, a most uniform temperature distribution on the external motor frame has been measured with respect to a still-rotor condition. It is an author's opinion that the internal air whirls contribute to reduce the temperature spread on the motor-frame surface.

In the proposed thermal model, the $R_{S-\mathrm{MF}}$ and $R_{S-\mathrm{EW}}$ are considered constant with reference to the rotor speed. This is reasonable, taking into account that these thermal resistances describe the thermal exchange inside massive materials and, in any case, the motor inner air does not influence their values.

Obviously, the $R_{\mathrm{EW}-\mathrm{MF}}$ thermal resistance depends on the rotor speed. This resistance can be considered as the parallel of three thermal resistances, as shown in the circle of Fig. 9.

In particular, it is possible to define the following thermal resistances:

1) R_{NC}: equivalent natural-convection thermal resistance between the endwinding and the motor frame (this resistance is the series of two contributions: the thermal resistance between the endwindings and the inner air and the thermal resistance between the inner air and the end caps);
2) R_{RAD}: radiation thermal resistance between the endwindings and the motor frame;
3) $R_{\mathrm{EW}-\mathrm{IA}}$: forced-convection thermal resistance between the endwindings and the end-space inner air;
4) $R_{\mathrm{IA}-\mathrm{MF}}$: forced-convection thermal resistance between the inner air and the motor frame.

The $R_{\mathrm{EW}-\mathrm{IA}}$ and $R_{\mathrm{IA}-\mathrm{MF}}$ resistances have to be considered infinite when the rotor is still because they are depending on the inner air whirls. In other words, when the rotor is still, only the natural convection and the radiation play a consistent role in the heat exchanges.

In order to identify the model thermal resistances, a multivariable minimization algorithm, available on Microsoft Excel, has been used. In accordance to a least square method, the algorithm is able to find the values of the $R_{S-\mathrm{EW}}$, $R_{\mathrm{EW}-\mathrm{MF}}$, and $R_{\mathrm{EW}-\mathrm{MF}}$ resistances that minimize the differences between the measured and computed overtemperatures in the whole rotor-speed range.

For the three prototypes, the numerical values of the thermal resistances are reported in Tables II–IV. In Tables V–VII, the relative percentage errors of the calculated overtemperatures are also shown. It is possible to observe that these errors are very small (lower than 1%).

TABLE II
MA160 PROTOTYPE: ESTIMATED THERMAL MODEL RESISTANCES

Thermal resistance [°C/W]	Rotor speed [r/min]						
	0	500	750	1000	1500	2000	2400
R_0	0.1656	0.1622	0.1585	0.1530	0.1359	0.1256	0.1255
$R_{S\text{-}MF}$	0.0846	0.0846	0.0846	0.0846	0.0846	0.0846	0.0846
$R_{S\text{-}EW}$	0.1562	0.1562	0.1562	0.1562	0.1562	0.1562	0.1562
$R_{EW\text{-}MF}$	0.2630	0.1776	0.1502	0.1187	0.0942	0.0815	0.0738
$R_{EW\text{-}IA} + R_{IA\text{-}MF}$	∞	0.5470	0.3505	0.2162	0.1468	0.1180	0.1026

TABLE III
MA132 PROTOTYPE: ESTIMATED THERMAL MODEL RESISTANCES

Relative error [%]	Rotor speed [r/min]						
	0	500	750	1000	1500	2000	2400
Slots	-0.12	0.06	-0.03	0.15	0.41	0.12	-0.61
Endwindings	-0.17	0.19	0.22	0.18	-0.05	-0.26	-0.35

TABLE IV
MA112 PROTOTYPE: ESTIMATED THERMAL MODEL RESISTANCES

	Rotor speed [r/min]						
	0	500	750	1000	1500	2000	2400
Heat flux [W]	-26	-13	-8.0	-1.0	+5.3	+8.9	+11.2

TABLE V
MA160 PROTOTYPE: ESTIMATED WINDING TEMPERATURE RELATIVE ERRORS

Thermal resistance [°C/W]	Rotor speed [r/min]						
	0	500	750	1000	1400	2000	2400
R_0	0.2233	0.2145	0.2049	0.2067	0.1856	0.1593	0.1531
$R_{S\text{-}MF}$	0.1080	0.1080	0.1080	0.1080	0.1080	0.1080	0.1080
$R_{S\text{-}EW}$	0	0	0	0	0	0	0
$R_{EW\text{-}MF}$	0.3867	0.2730	0.2406	0.2267	0.1581	0.1495	0.1259
$R_{EW\text{-}IA} + R_{IA\text{-}MF}$	∞	0.9287	0.6371	0.5479	0.2674	0.2436	0.1866

TABLE VI
MA132 PROTOTYPE: ESTIMATED WINDING TEMPERATURE RELATIVE ERRORS

Relative error [%]	Rotor speed [r/min]						
	0	500	750	1000	1400	2000	2400
Winding (average)	-0.28	0.20	0.17	0.13	0.08	-0.10	-0.29

For the MA132 and MA112 prototypes, the algorithm enforces at zero the $R_{S-\mathrm{EW}}$ thermal resistance. This is correct, because for these two prototypes, the endwindings are at the same temperature as of the copper embedded in the slots. Obviously, this does not mean that the heat flux between these two winding parts (Tables VIII and IX) is not actually present.

As a general remark, the minimization algorithm convergence depends on the initial choice of the thermal-resistance values. In particular, a more stable numerical solution has been obtained constraining the regression line of the forced-convection heat-transfer coefficient ($h_{\mathrm{Forced\ convection}}$, see Section VI) to cross the axis origin when the rotor is still. In any case, the proposed thermal resistances verify all the physical phenomena observed in the measurements, such as the heat flow presence between the endwindings and the copper embedded in the slot (Tables VIII–X).

TABLE VII
MA112 PROTOTYPE: ESTIMATED WINDING TEMPERATURE RELATIVE ERRORS

	Rotor speed [r/min]						
	0	500	750	1000	1400	2000	2400
Heat flux [W]	-41	-30	-26	-23	-9.3	-6.9	0.3

TABLE VIII
MA132 PROTOTYPE: ESTIMATED SLOT-TO-ENDWINDING HEAT FLUX

Thermal resistance [°C/W]	Rotor speed [r/min]						
	0	500	750	1000	1400	2000	2400
R_0	0.2787	0.2714	0.2749	0.2582	0.2784	0.2782	0.2776
$R_{S\text{-}MF}$	0.1431	0.1431	0.1431	0.1431	0.1431	0.1431	0.1431
$R_{S\text{-}EW}$	0	0	0	0	0	0	0
$R_{EW\text{-}MF}$	0.4872	0.3690	0.3411	0.2344	0.2177	0.1755	0.1701
$R_{EW\text{-}IA} + R_{IA\text{-}MF}$	∞	1.5209	1.1382	0.4518	0.3934	0.2744	0.2615

TABLE IX
MA112 PROTOTYPE: ESTIMATED SLOT-TO-ENDWINDING HEAT FLUX

Relative error [%]	Rotor speed [r/min]						
	0	500	750	1000	1400	2000	2400
Winding (average)	1.36	-0.96	-0.78	-0.75	-0.32	0.43	1.02

TABLE X
MA160 PROTOTYPE: ESTIMATED SLOT-TO-ENDWINDING HEAT FLUX

	Rotor speed [r/min]						
	0	500	750	1000	1400	2000	2400
Heat flux [W]	-43	-36	-34	-23	-20	-13	-11

In this paper, as the first approximation, the R_{NC} and the R_{RAD} are considered constant with the rotor speed. This hypothesis allows the separation between the forced-convection contribution and the others. In fact, for any rotor speed (n), it is possible to evaluate the series of $R_{\mathrm{EW-IA}}$ and $R_{\mathrm{IA-MF}}$ thermal resistances, as shown in the following expression:

$$R_{\mathrm{EW-IA}} + R_{\mathrm{IA-MF}} = 1 \Big/ \left(\frac{1}{R_{\mathrm{EW-MF}}} - \frac{1}{R_{\mathrm{EW-MF}}|_{n=0}} \right). \tag{3}$$

The forced-convection thermal resistances are reported in the last row of Tables II–IV, respectively, for the three prototypes.

From Figs. 10–12, the equivalent thermal resistances between the endwindings and the motor frame $(R_{\mathrm{EW-MF}})$, together with the forced-convection contributions ($R_{\mathrm{EW-IA}}$ plus $R_{\mathrm{IA-MF}}$) versus the rotor speed are shown.

VI. HEAT-TRANSFER COEFFICIENTS

Starting from the thermal resistances and the involved surfaces, the heat-transfer coefficients can be determined by (2). The selection of the involved surface values is not a simple task. In this paper, the surfaces shown in Fig. 13 have been taken into account. In the first approximation, the endwindings surface S_{EW} has been evaluated by the following expression:

$$S_{\mathrm{EW}} = 2\frac{\pi}{2} P_{\mathrm{EW}} D_{\mathrm{EW}} \tag{4}$$

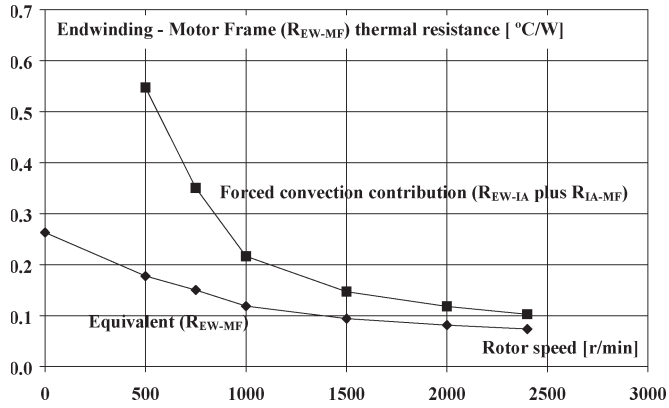

Fig. 10. Endwindings–motor-frame thermal resistances versus the rotor speed (MA160 motor prototype).

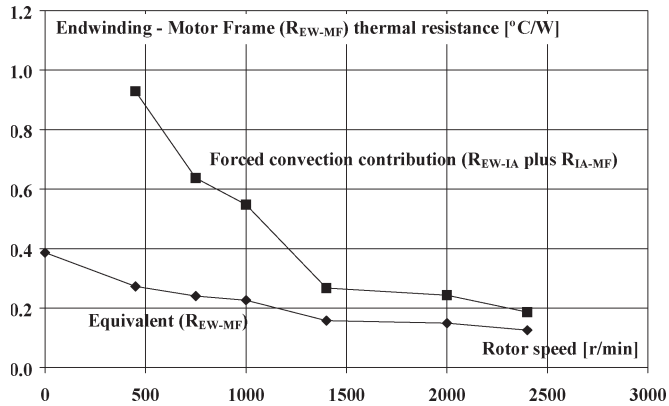

Fig. 11. Endwindings–motor-frame thermal resistances versus the rotor speed (MA132 motor prototype).

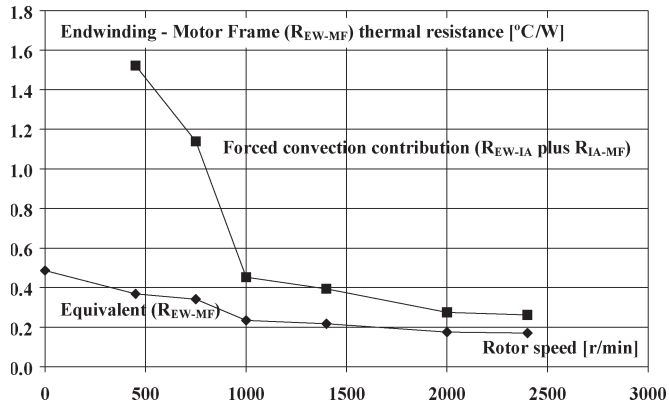

Fig. 12. Endwindings–motor-frame thermal resistances versus the rotor speed (MA112 motor prototype).

where P_{EW} is the endwinding perimeter, and D_{EW} is the endwinding average diameter (Table I).

Since this surface is not smooth (because the windings are typically constituted by wire), a corrective coefficient of $\pi/2$ has been adopted in (4). It is important to underline that, by the thermal resistance point of view, the two end-space regions have to be considered in parallel. This fact is taken in account by the multiplication by two in (4).

For the inner end-cap surface S_{EC}, a general equation cannot be "*a priori*" defined because this surface depends on the actual end-cap shape, so this surface has to be measured case by case. The surfaces reported in Fig. 13 are the surfaces of the two endwindings and the inner surface of the two end caps.

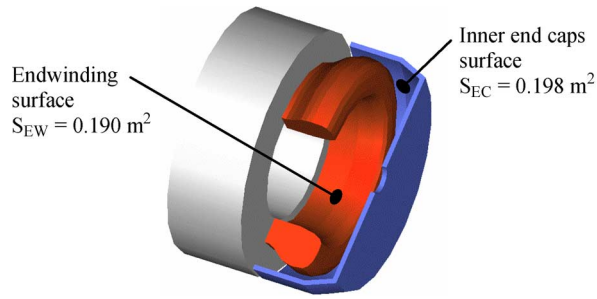

Fig. 13. Surfaces involved in the heat-transfer-coefficient estimation (the values are referred to the MA160 prototype).

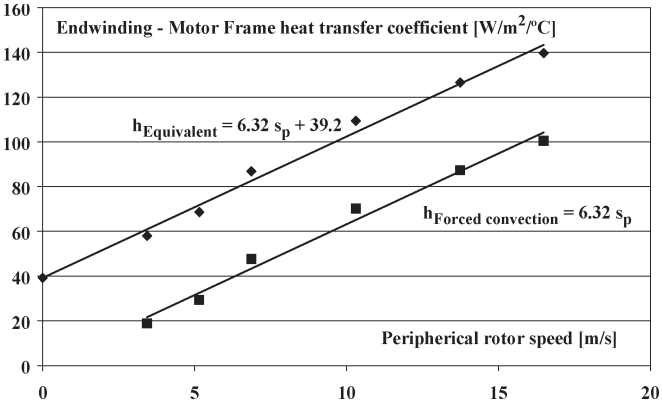

Fig. 14. Estimated heat-transfer coefficients versus the peripheral rotor speed (s_p in meters per second) for the MA160 prototype.

Assuming that the heat-transfer coefficients between the endwindings and the inner air and between the inner air and the end caps are equal, the following equations can be defined:

$$h_{\mathrm{Equivalent}} = \frac{1}{R_{\mathrm{EW-MF}}}\left(\frac{1}{S_{\mathrm{EW}}} + \frac{1}{S_{\mathrm{EC}}}\right) \tag{5}$$

$$h_{\mathrm{ForcedConvection}} = \frac{1}{R_{\mathrm{EW-IA}} + R_{\mathrm{IA-MF}}}\left(\frac{1}{S_{\mathrm{EW}}} + \frac{1}{S_{\mathrm{EC}}}\right). \tag{6}$$

The $h_{\mathrm{Equivalent}}$ heat-transfer coefficient takes into account all the heat-exchange phenomena that occur in the end-space regions (natural convection, radiation, and forced convection). As a consequence, this coefficient can be compared with the published ones (see Fig. 1).

The $h_{\mathrm{Forced\ Convection}}$ coefficient describe only the heat transfer related to the forced-convection contribution. This coefficient can be computed using the data reported in the last row of Tables II–IV, with exception of the point at zero rotor speed.

The obtained results are reported from Figs. 14–16 as function of the peripheral rotor speed. In the same figures, the regression lines of the computed data are also reported. The agreement between the heat-transfer-coefficient values reported in Fig. 1 and the estimated $h_{\mathrm{Equivalent}}$ ones is good, as shown in Fig. 17.

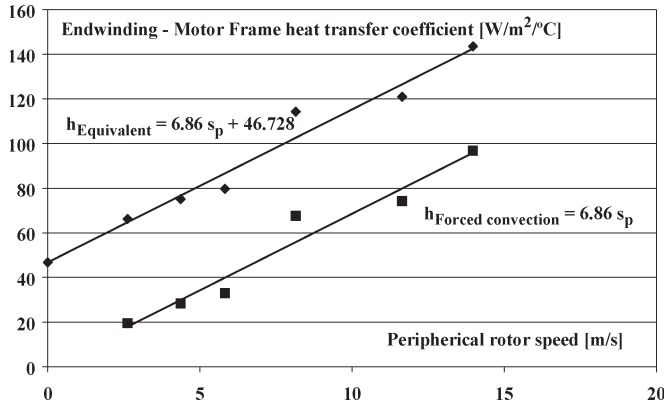

Fig. 15. Estimated heat-transfer coefficients versus the peripheral rotor speed (s_p in meters per second) for the MA132 prototype.

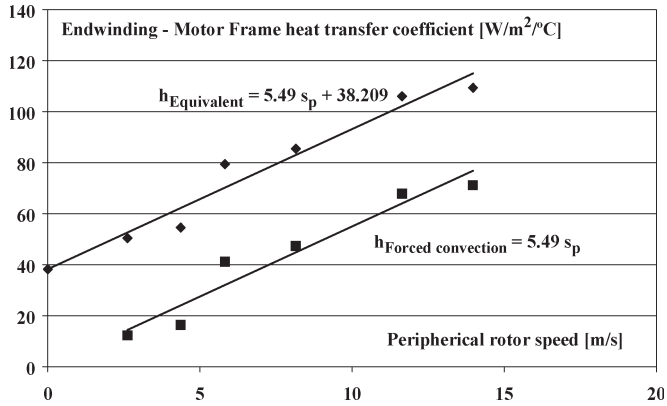

Fig. 16. Estimated heat-transfer coefficients versus the peripheral rotor speed (s_p in meters per second) for the MA112 prototype.

It is interesting to observe that the $h_{\text{Forced Convection}}$ results equal to zero when the rotor is still because the forced-convection thermal path is not active in this condition (see Fig. 9).

VII. Final Considerations

Taking into account the results reported in Figs. 14–16, the following considerations can be done.

1) In the considered speed range, for each prototype, a linear dependence of the heat-transfer coefficients versus the inner air speed has been found.
2) For the MA160 and MA132 motor prototypes, the obtained heat-transfer-coefficient values are comparable. This means that the inner ventilation play a similar role in the endwinding cooling, even if the endwinding enlargement in the end-space regions is quite different [Fig. 3(b) and (c)].
3) For the MA112, a lower influence of the air whirls on the heat-transfer coefficients has been found. In any case, when the rotor is still and the inner forced ventilation is not active, the $h_{\text{Equivalent}}$ coefficient confirms the results obtained for the other two prototypes and the result published in the technical literature (Fig. 1). It is important to remember that MA112 prototype is the smallest one and the endwinding length is greater than the stator-core length (Table I).
4) In addition, the insulation cylinder mounted under the shaft-side endwinding [Fig. 3(a)] introduces a not negligible conduction thermal path between the endwindings and the external case. The simplified prototypes thermal model takes into account the heat flow in this path as an equivalent heat flux in the endwindings–slots-motor frame thermal path. As a consequence, it is reasonable that, for the MA112 prototypes, the "average effect" of the inner ventilation at high speed (in other words, the angular coefficient of the regression line $h_{\text{Forced convection}}$) is lower than the MA160 and MA132 prototype.
5) The measurement data highlight that the inner ventilation is more efficient for a motor with more free space around the endwindings.
6) Fig. 17 shows a good correlation between the new experimental values and the curves proposed in the technical literature. Using the obtained results, for motors with sizes and endwinding geometries similar to the considered prototypes, a forced-convection coefficient can be computed using

$$h = 6.22v. \tag{7}$$

In order to combine in a single equivalent heat-exchange coefficient, both the natural- and forced-convection phenomena, (7) can be modified. as shown as follows:

$$h = 41.4 + 6.22v. \tag{8}$$

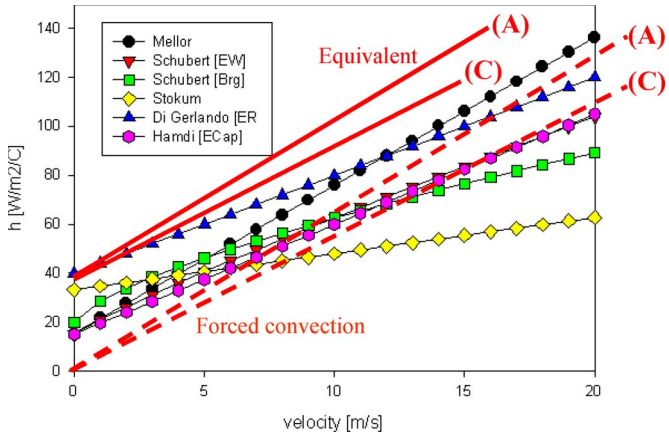

Fig. 17. Comparison between the estimated heat-transfer coefficients with the published ones. (A) MA160 motor prototype; (C) MA112 motor prototype.

VIII. Conclusion

In this paper, the internal air cooling effects on the endwinding temperature have been analyzed using an experimental approach. Three suitable motor prototypes with a plastic rotor core have been built and tested. The measurement results have shown that all the motor-part overtemperatures (winding, endwindings, stator lamination, and external motor frame) decrease, with the inner air speed increase. In particular, for the stator winding, an overtemperature decreasing up to 15 °C has

been observed. The authors propose a simplified thermal model suitable to describe the thermal behaviors of the prototypes. In this paper, the complete procedure for the model thermal-resistance identification is reported in detail. In particular, the proposed procedure allows separating the forced-convection contribution by the other thermal-exchange phenomena that occur in the end-space regions. The obtained heat-transfer coefficients are in agreement with the results reported in the past literature. Finally, a critical analysis of the results has been carried out.

ACKNOWLEDGMENT

The authors would like to thank Fimet Motori and Riduttori for the technical support of this research.

REFERENCES

[1] S. K. Pal, "Heat transfer in electrical machines—A critical review," Electrical Assoc. Rep., ERA Technology Limited, Project 5182/5, Jul. 1971.
[2] E. Schubert, "Heat transfer coefficients at end-winding and bearing covers of enclosed asynchronous machines," *Elektrie*, vol. 22, Apr. 1968.
[3] G. E. Luke, "The cooling of electrical machine," *Trans. AIEEE*, vol. 42, pp. 636–652, 1923.
[4] K. Takahashi, H. Kuwahara, K. Kajiwara, and T. Obata, "Airflow and thermal conductance in totally enclosed induction motor," *Heat Transf.—Asian Res.*, vol. 31, no. 1, pp. 7–20, 2002.
[5] D. A. Staton, A. Boglietti, and A. Cavagnino, "Solving the more difficult aspects of electric motor thermal analysis," in *Proc. IEMDC Conf.*, Madison, WI, Jun. 1–4, 2003, pp. 747–755.
[6] A. Boglietti, M. Cavagnino, M. Lazzari, and M. Pastorelli, "A simplified thermal model for variable speed self cooled industrial induction motor," *IEEE Trans. Ind. Appl.*, vol. 39, no. 4, pp. 945–952, Jul./Aug. 2003.
[7] P. H. Mellor, D. Roberts, and D. E. Turner, "Lumped parameter thermal model for electrical machines of TEFC design," *Proc. Inst. Electr. Eng.*, vol. 138, no. 5, pt. B, pp. 205–218, Sep. 1991.
[8] A. DiGerlando and I. Vistoli, "Thermal networks of induction motors for steady state and transient operation analysis," in *Proc. ICEM Conf.*, Paris, France, Sep. 5–8, 1994, pp. 452–457.
[9] G. Stokum, "Use of the results of the four-heat run method of induction motors for determining thermal resistance," *Elektrotechnika*, vol. 62, no. 6, pp. 219–232, 1969.
[10] E. S. Hamdi, *Design of Small Electrical Machines*. Hoboken, NJ: Wiley, 1994.
[11] D. Staton, "Thermal analysis of electric motors and generators," presented at the IEEE IAS Annu. Meeting, Chicago, IL, 2001. Tutorial Course Notes.
[12] A. Boglietti, A. Cavagnino, and D. Staton, "Thermal analysis of TEFC induction motors," in *Proc. IEEE Ind. Appl. Soc. Annu. Meeting*, Salt Lake City, UT, Oct. 12–16, 2003, pp. 849–856.

Aldo Boglietti (M'04–SM'06) was born in Rome, Italy, in 1957. He received the Laurea degree in electrical engineering from the Politecnico di Torino, Turin, Italy, in 1981.

He started his research work with the Department of Electrical Engineering, Politecnico di Torino, as a Researcher of electrical machines in 1984, becoming an Associate Professor of electrical machines in 1992, and a Full Professor in November 2000. He is the Head of the Electrical Engineering Department, Politecnico of Torino, until 2007. He has authored about 100 papers, and his research interests include the energetic problem in electrical machines and drives, high-efficiency industrial motors, magnetic materials and their applications in electrical machines, electrical machine and drive models, and thermal problems in electrical machines.

Andrea Cavagnino (M'04) was born in Asti, Italy, in 1970. He received the M.Sc. and Ph.D. degrees in electrical engineering from the Politecnico di Torino, Turin, Italy, in 1995 and 1999, respectively.

In 1997, he joined the Electrical Machines Laboratory, Department of Electric Engineering, Politecnico di Torino, where he is currently an Assistant Professor. His fields of interest include electromagnetic design, thermal design, and energetic behaviors of electric machines. He has authored several papers published in technical journals and conference proceedings.

Dr. Cavagnino is a Registered Professional Engineer in Italy.